Inorg. Chem. **2006**, *45*, 4440–4447

Importance of the O–M–O Bridges (M = V^{5+}, Mo^{6+}) for the Spin-Exchange Interactions in the Magnetic Oxides of Cu^{2+} Ions Bridged by MO_4 Tetrahedra: Spin-Lattice Models of $Rb_2Cu_2(MoO_4)_3$, $BaCu_2V_2O_8$, and $KBa_3Ca_4Cu_3V_7O_{28}$

Hyun-Joo Koo*

Department of Chemistry and Research Institute of Basic Science, Kyung Hee University, Seoul 130-701, South Korea

Myung-Hwan Whangbo*

Department of Chemistry, North Carolina State University, Raleigh, North Carolina 27695-8204

Received March 8, 2006

The spin-lattice models relevant for the magnetic oxides $Rb_2Cu_2(MoO_4)_3$, $BaCu_2V_2O_8$, and $KBa_3Ca_4Cu_3V_7O_{28}$ were determined by evaluating the relative strengths of the spin-exchange interactions between their Cu^{2+} ions on the basis of spin dimer analysis. Our study shows that the O–M–O bridges (M = V^{5+}, Mo^{6+}) between the magnetic ions Cu^{2+}, provided by the MO_4 tetrahedra, are crucial for the spin-exchange interactions and hence for deducing the spin-lattice models needed to interpret the magnetic properties of these oxides. The spin-lattice model of $Rb_2Cu_2(MoO_4)_3$ is not a uniform chain but two interpenetrating spin ladders that interact weakly with geometric spin frustration. The spin-lattice model of $BaCu_2V_2O_8$ is an alternating chain as expected, but the spin-exchange paths responsible for it differ from those expected. With respect to the strongest spin exchange of $BaCu_2V_2O_8$, the spin exchange of $KBa_3Ca_4Cu_3V_7O_{28}$ is only slightly weaker, but the strongest spin exchange of $Rb_2Cu_2(MoO_4)_3$ is much weaker. This difference in the spin-exchange strengths is caused by the difference in the bridging modes of the MO_4 tetrahedra leading to these spin-exchange interactions.

1. Introduction

To interpret the magnetic properties of a given magnetic system, one needs a spin-lattice model (i.e., the repeat patterns of strongly interacting spin-exchange paths) with which to analyze the magnetic data so that the evaluation of the relative strengths of its spin-exchange interactions becomes necessary.[1] In a magnetic oxide of spin $^1/_2$ Cu^{2+} ions, spin-exchange interactions between adjacent ions are either superexchange (SE) interactions involving Cu−O−Cu paths[2] or super-superexchange (SSE) interactions involving Cu−O···O−Cu paths.[1,3] SSE interactions can be much stronger than SE interactions[1,3] but have frequently been neglected without justifiable reasons. To find a spin-lattice model relevant for a magnetic oxide, the relative strengths of both SE and SSE interactions should be evaluated on the basis of proper electronic structure considerations. The quantitative evaluation of spin-exchange interactions requires first principles electronic structure calculations for molecular clusters representing spin dimers with either the configuration interaction wave function or the density functional theory method[4] or first principles electronic band structure calculations for crystalline solids.[5] In identifying a correct set of

* To whom correspondence should be addressed. E-mail: hjkoo@khu.ac.kr (H.-J.K.), mike_whangbo@ncsu.edu (M.-H.W.).

(1) For reviews, see: (a) Whangbo, M.-H.; Koo, H.-J.; Dai, D. *J. Solid State Chem.* **2003**, *176*, 417. (b) Whangbo, M.-H.; Dai, D.; Koo, H.-J. *Solid State Sci.* **2005**, *7*, 827.

(2) Goodenough, J. B. *Magnetism and the Chemical Bond*; Wiley: Cambridge, MA, 1963.

(3) (a) Koo, H.-J.; Whangbo, M.-H. *Inorg. Chem.* **2001**, *40*, 2169. (b) Koo, H.-J.; Whangbo, M.-H.; VerNooy, P. D.; Torardi, C. C.; Marshall, W. J. *Inorg. Chem.* **2002**, *41*, 4664. (c) Whangbo, M.-H.; Koo, H.-J.; Dai, D.; Jung, D. *Inorg. Chem.* **2003**, *42*, 3898. (d) Koo, H.-J.; Whangbo, M.-H.; Lee, K.-S. *Inorg. Chem.* **2003**, *42*, 5932. (e) Koo, H.-J.; Dai, D.; Whangbo, M.-H. *Inorg. Chem.* **2005**, *44*, 4359.

(4) (a) Illas, F.; Moreira, I. de P. R.; de Graaf, C.; Barone, V. *Theor. Chem. Acc.* **2000**, *104*, 265 and references cited therein. (b) Illas, F.; Moreira, I. de P. R.; Bofill, J. M.; Filatov, M. *Phys. Rev. B* **2004**, *70*, 132414. (c) Ruiz, E.; Rodriguez-Fortea, A.; Cano, J.; Alvarez, S. *J. Phys. Chem. Solids* **2004**, *65*, 799.

10.1021/ic060392w CCC: $33.50
Published on Web 04/28/2006

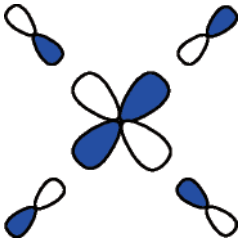

Figure 1. Magnetic orbital of a $Cu(O_{eq})_4$ square plane.

spin-exchange paths to analyze experimental data and hence correctly explaining the physical properties of a magnetic solid, it is often sufficient to know the relative strengths of its spin-exchange interactions.[1,3] For this qualitative purpose, the spin dimer analysis based on extended Hückel tight binding (EHTB) calculations has been indispensable for a variety of magnetic oxides,[1,3] because it reproduces the relative strengths of spin-exchange interactions determined from first principles electronic structure calculations.[1,3]

Spin-exchange interactions in magnetic oxides of spin $^1/_2$ Cu^{2+} ions are strongly governed by the arrangements of their CuO_4 square planes containing the magnetic orbitals.[1,3] For the convenience of our discussion, such CuO_4 square planes will be referred to as the $Cu(O_{eq})_4$ square planes. In the magnetic orbital of a $Cu(O_{eq})_4$ square plane, the Cu $3d_{x^2-y^2}$ orbital makes σ antibonding with the 2p orbitals of the four O_{eq} atoms (Figure 1). A crucial factor determining the strength of a spin-exchange interaction between Cu^{2+} ions is not the Cu $3d_{x^2-y^2}$ orbitals but the O 2p orbitals of their magnetic orbitals (i.e., the "tails" of the magnetic orbitals) because the spin exchange between two adjacent Cu^{2+} ions depends on the overlap between their magnetic orbitals, which is, in turn, determined by the overlap between their tails.[1,3] For phosphates of Cu^{2+} ions, in which the $O_{eq}\cdots O_{eq}$ contacts of the $Cu-O_{eq}\cdots O_{eq}-Cu$ spin-exchange paths are provided by PO_4 tetrahedra, the spin dimer analysis based on EHTB calculations showed that the relative strengths of the SE and SSE interactions are not strongly affected by whether the PO_4 tetrahedral units are included in the spin dimers representing the spin-exchange interactions.[1,3b,e,6] (An exception was recently found for the spin-gap systems α-$AgCuPO_4$ and β-$AgCuPO_4$.[7] For further discussion, see section 6.) This reflects the fact that the 3s3p orbitals of P do not contribute strongly in the energy region of the magnetic orbitals of the $Cu(O_{eq})_4$ square planes. This may not be the case if the $O_{eq}\cdots O_{eq}$ contacts of $Cu-O_{eq}\cdots O_{eq}-Cu$ spin-exchange paths are provided by VO_4 tetrahedra containing V^{5+} (d^0) ions or by MoO_4 tetrahedra containing Mo^{6+} (d^0) ions because the V 3d orbitals and the Mo 4d orbitals can contribute substantially in the energy region of the magnetic orbitals of the $Cu(O_{eq})_4$ square planes. Indeed, our study of $LiCuVO_4$ showed that SSE interactions between Cu^{2+} ions are strongly affected by the bridging VO_4 units.[8]

The present study deals with the spin-exchange interactions in the three oxides of Cu^{2+} ions in which the magnetic ions are bridged by VO_4 and MoO_4 tetrahedra, namely, $Rb_2Cu_2(MoO_4)_3$,[9−11] $BaCu_2V_2O_8$,[12−16] and $KBa_3Ca_4Cu_3V_7O_{28}$.[17,18] For a magnetic oxide with simple crystal structure such as $KBa_3Ca_4Cu_3V_7O_{28}$, its spin-lattice model can be deduced by simply inspecting the arrangement of its magnetic ions. For magnetic oxides with complex crystal structures such as $Rb_2Cu_2(MoO_4)_3$ and $BaCu_2V_2O_8$, however, it is difficult to deduce their spin-lattice models unless proper electronic structure considerations are taken into account. In the present work, we evaluate the relative strengths of the SE and SSE interactions of $Rb_2Cu_2(MoO_4)_3$, $BaCu_2V_2O_8$, and $KBa_3Ca_4Cu_3V_7O_{28}$ by performing spin dimer analysis based on EHTB calculations.[19,20] Our work reveals the importance of SSE interactions mediated by the O−M−O bridges (M = V^{5+}, Mo^{6+}) in finding the spin-lattice models relevant for magnetic oxides of Cu^{2+} ions bridged by MO_4 tetrahedra.

2. Spin Dimer Analysis

The strength of a spin-exchange interaction between two spin sites is described by a spin-exchange parameter $J = J_F + J_{AF}$, where J_F is the ferromagnetic (FM) term ($J_F > 0$) and J_{AF} is the antiferromagnetic (AFM) term ($J_{AF} < 0$). In most cases, J_F is very small so that the trends in the J values are well approximated by those in the corresponding J_{AF} values.[1,3] For a spin dimer in which each spin site contains one unpaired spin, the J_{AF} term is approximated by[1]

$$J_{AF} \approx -(\Delta\epsilon)^2/U_{eff} \qquad (1)$$

where U_{eff} is the effective on-site repulsion, which is essentially a constant for a given compound. If the two spin sites are equivalent, $\Delta\epsilon$ is the energy difference Δe between the two magnetic orbitals representing the spin dimer. When the two spin sites are nonequivalent, $(\Delta\epsilon)^2 = (\Delta e)^2 - (\Delta e^0)^2$, where Δe^0 is the energy difference between the magnetic orbitals representing each spin site of the spin dimer ($\Delta e^0 =$

(5) (a) Chartier, A.; D'Arco, P.; Dovesi, R.; Saunders, V. R. *Phys. Rev. B* **1999**, *60*, 14042 and references cited therein. (b) Dai, D.; Whangbo, M.-H.; Koo, H.-J.; Rocquefelte, X.; Jobic, S.; Villesuzanne, A. *Inorg. Chem.* **2005**, *44*, 2407.
(6) Belik, A. A.; Azuma, M.; Matsuo, A.; Whangbo, M.-H.; Koo, H.-J.; Kikuchi, J.; Kaji, T.; Okubo, S.; Ohta, H.; Kindo, K.; Takano, M. *Inorg. Chem.* **2005**, *44*, 6632.
(7) The strongest spin-exchange interaction in each of these two phosphates is an SSE interaction, which becomes negligible if the bridging PO_4 units are omitted. See: Ben Yahia, H.; Gaudin, E.; Darriet, J.; Whangbo, M.-H. *Inorg. Chem.* **2006**, submitted for publication.
(8) Dai, D.; Koo, H.-J.; Whangbo, M.-H. *Inorg. Chem.* **2004**, *43*, 4026.
(9) Solodovnikov, S. F.; Solodovnikova, Z. A. *J. Struct. Chem.* **1997**, *38*, 765.
(10) Hase, M.; Kuroe, H.; Ozawa, K.; Suzuki, O.; Kitazawa, H.; Kido, G.; Sekine, T. *Phys. Rev. B* **2004**, *70*, 104426.
(11) Hase, M.; Ozawa, K.; Suzuki, S.; Kitazawa, H.; Kido, G.; Kuroe, H.; Sekine, T. *J. Appl. Phys.* **2005**, *97*, 10B303.
(12) Vogt, R.; Müller-Buschbaum, Hk. *Z. Anorg. Allg. Chem.* **1990**, *591*, 167.
(13) Sakurai, H.; Yoshimura, K.; Kosuge, K. *J. Phys. Soc. Jpn.* **2002**, *71* (Suppl.), 190.
(14) He, Z.; Kyômen, T.; Itoh, M. *Phys. Rev. B* **2004**, *69*, 220407.
(15) Ghoshray, K.; Pahari, B.; Bndyopadhyay, B.; Sarkar, R.; Ghoshray, A. *Phys. Rev. B* **2005**, *71*, 214401.
(16) Lue, C. S.; Xie, B. X. *Phys. Rev. B* **2005**, *72*, 52409.
(17) von Postel, M.; Müller-Buschbaum, Hk. *Z. Anorg. Allg. Chem.* **1993**, *619*, 123.
(18) Sakurai, H.; Yoshimura, K.; Kosuge, K.; Ishikawa, F.; Mitamura, H.; Goto, T. *J. Phys. Soc. Jpn.* **2002**, *71*, 664.
(19) Hoffmann, R. *J. Chem. Phys.* **1963**, *39*, 1397.
(20) Our calculations were carried out by employing the SAMOA (Structure and Molecular Orbital Analyzer) program package (Dai, D.; Ren, J.; Liang, W.; Whangbo, M.-H., http://chvamw.chem.ncsu.edu/, 2002).

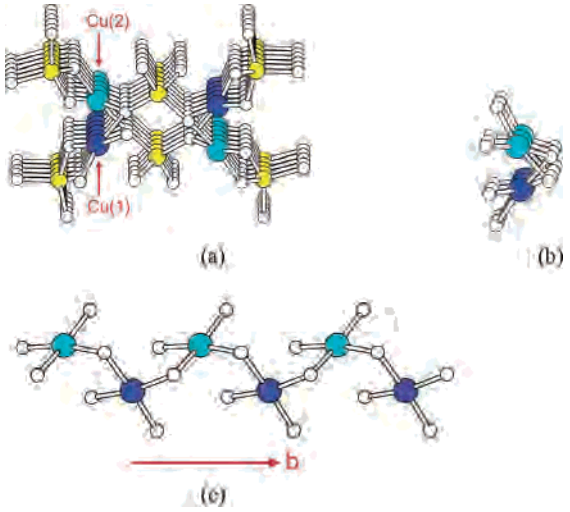

Figure 2. Building blocks of $Rb_2Cu_2(MoO_4)_3$: (a) projection view of a $[Cu_2(MoO_4)_3]^{2-}$ chain; (b) projection view of a corner-sharing $Cu(O_{eq})_3$ chain; (c) perspective view of a corner-sharing $Cu(O_{eq})_3$ chain. The blue and cyan circles represent Cu(1) and Cu(2) atoms, respectively, the yellow circles the Mo atoms, and the white circles the O atoms.

0 if the two spin sites are equivalent). Because the magnetic orbitals of Cu^{2+} ions are contained in their $Cu(O_{eq})_4$ square planes, important spin-exchange paths between adjacent Cu^{2+} ions are those involving the $Cu-O_{eq}$ bonds from both ions, i.e., the $Cu-O_{eq}-Cu$ and $Cu-O_{eq}\cdots O_{eq}-Cu$ spin-exchange paths. In the present work, the Δe and Δe^0 values for various spin dimers are evaluated by performing EHTB calculations. For a variety of magnetic solids of transition-metal ions, it has been found[1,3] that their magnetic properties are well described by the $(\Delta\epsilon)^2$ values obtained from EHTB calculations, when both the d orbitals of the transition-metal ions and the s/p orbitals of its surrounding ligands are represented by double-ζ Slater-type orbitals.[21] Our calculations are carried out using the atomic parameters summarized in Table S1 of the Supporting Information.

3. Spin Lattice of $Rb_2Cu_2(MoO_4)_3$

$Rb_2Cu_2(MoO_4)_3$ has two nonequivalent Cu atoms, Cu(1) and Cu(2), and consists of $[Cu_2(MoO_4)_3]^{2-}$ chains (Figure 2a) separated by Rb^+ ions.[9] Each $[Cu_2(MoO_4)_3]^{2-}$ chain contains two $Cu(O_{eq})_3$ chains in which corner-sharing $Cu(1)(O_{eq})_4$ and $Cu(2)(O_{eq})_4$ square planes alternate (Figure 2b,c). In each $Cu(O_{eq})_3$ chain, every shared O_{eq} atom is provided by a MoO_4 tetrahedron and every pair of next-nearest-neighbor Cu^{2+} ions is bridged by a MoO_4 tetrahedron (Figure 3a). On the basis of this structural feature, Hase et al.[10,11] interpreted the magnetic susceptibility data of $Rb_2Cu_2(MoO_4)_3$ in terms of a uniform Heisenberg chain model

$$\hat{H} = -\sum_{i=1}^{N}(J_1\hat{S}_i\cdot\hat{S}_{i+1} + J_2\hat{S}_i\cdot\hat{S}_{i+2}) \qquad (2)$$

with the nearest-neighbor spin exchange J_1 and the next-nearest-neighbor spin exchange J_2 (Figure 3b). The fitting analysis[10,11] of the magnetic susceptibility data using this model between 15 and 140 K led to $J_1/k_B = 138$ K and $J_2/k_B = -51$ K. Thus, this model predicts that the dominant spin-exchange interaction is FM (i.e., $J_1 > 0$). The experimental magnetic susceptibility of $Rb_2Cu_2(MoO_4)_3$ shows a maximum at ~14 K and decreases with decreasing temperature below ~14 K. However, the calculated magnetic susceptibility using the uniform chain model keeps on increasing below 14 K, so that this model cannot be correct. To predict the occurrence of a magnetic susceptibility maximum, the dominant spin-exchange interaction of $Rb_2Cu_2(MoO_4)_3$ should be AFM instead of FM.

It should be noted that the two $Cu(O_{eq})_3$ chains in a $[Cu_2(MoO_4)_3]^{2-}$ chain are bridged by MoO_4 tetrahedra (Figure 4a,b). The uniform chain model of Figure 3b neglects

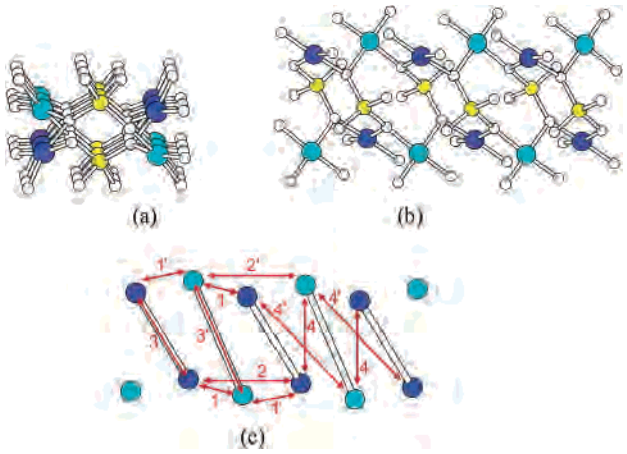

Figure 4. (a) Projection and (b) perspective views of two adjacent corner-sharing $Cu(O_{eq})_3$ chains bridged by MoO_4 tetrahedra. (c) Various spin-exchange paths of $Rb_2Cu_2(MoO_4)_3$, where the numbers 1, 1′, 2, 2′, 3, 3′, 4, and 4′ refer to the spin-exchange paths J_1, J_1', J_2, J_2', J_3, J_3', J_4, and J_4', respectively.

the possibility of strong spin-exchange interactions between the two $Cu(O_{eq})_3$ chains through the bridging MoO_4 tetrahedra and the presence of two nonequivalent Cu atoms in each $Cu(O_{eq})_3$ chain. Between the two $Cu(O_{eq})_3$ chains, there occur pairs of $Cu(1)(O_{eq})_4$ square planes that are nearly parallel to each other and bridged by two MoO_4 tetrahedra and so do such pairs of $Cu(2)(O_{eq})_4$ square planes (Figure

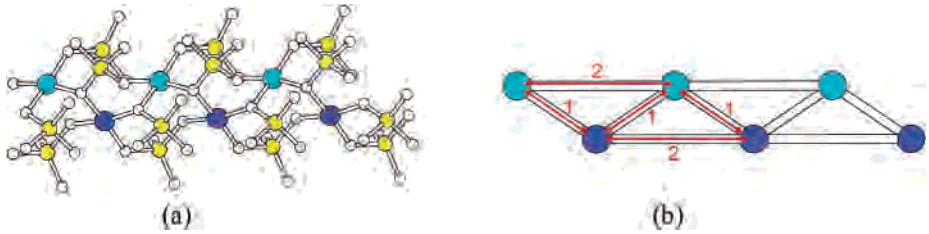

Figure 3. (a) Perspective view of a corner-sharing $Cu(O_{eq})_3$ chain with bridging MoO_4 tetrahedra. (b) Uniform chain model proposed for $Rb_2Cu_2(MoO_4)_3$ by Hase et al.,[11] where the numbers 1 and 2 refer to the spin-exchange interactions J_1 and J_2, respectively.

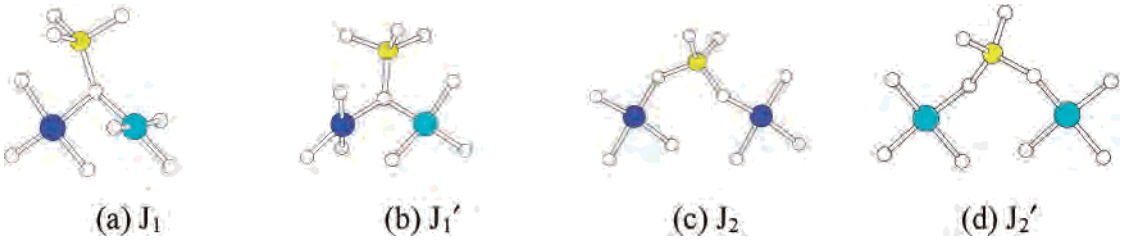

Figure 5. Intrachain spin dimers of $Rb_2Cu_2(MoO_4)_3$ associated with the spin-exchange paths (a) J_1, (b) J_1', (c) J_2, and (d) J_2'.

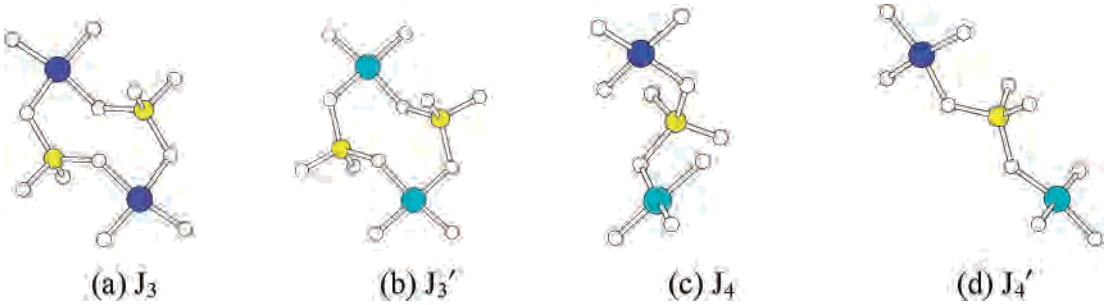

Figure 6. Interchain spin dimers of $Rb_2Cu_2(MoO_4)_3$ associated with the spin-exchange paths (a) J_3, (b) J_3', (c) J_4, and (d) J_4'.

Table 1. Geometrical Parameters and $(\Delta\epsilon)^2$ Values Associated with the Spin-Exchange Paths in $Rb_2Cu_2(MoO_4)_3$[a]

(a) SE Interactions

path	between	Cu···Cu	∠Cu−O−Cu	$(\Delta\epsilon)^2$
J_1	Cu(1)/Cu(2)	3.077	101.8	640 (0.31)[b]
J_1'	Cu(1)/Cu(2)	3.087	101.1	570 (0.27)

(b) SSE Interactions

path	between	Cu···Cu	O···O	∠Cu−O···O	$(\Delta\epsilon)^2$
			Intrachain		
J_2	Cu(1)/Cu(1)	5.102	2.719	141.8, 107.0	830 (0.40)
			2.964	98.4, 129.3	
J_2'	Cu(2)/Cu(2)	5.102	2.643	107.0, 145.6	1290 (0.62)
			2.966	98.5, 133.9	
			Interchain		
J_3	Cu(1)/Cu(1)	5.681	3.230	95.5, 155.8	2080 (1.00)
			3.230	95.5, 155.8	
J_3'	Cu(2)/Cu(2)	5.795	3.230	102.3, 161.9	1710 (0.82)
			3.230	102.3, 161.9	
J_4	Cu(1)/Cu(2)	4.911	3.230	95.5, 102.3	380 (0.18)
J_4'	Cu(1)/Cu(2)	6.984	3.230	155.8, 161.9	330 (0.16)

[a] The bond lengths are in Å units, the bond angles are in degrees, and the $(\Delta\epsilon)^2$ values are in $(meV)^2$ units. [b] The relative values of $(\Delta\epsilon)^2$ are given in parentheses.

4b). The arrangement of these pairs is schematically depicted in Figure 4c by representing each pair as a dumbbell connecting its two Cu^{2+} ions. The various spin-exchange paths of $Rb_2Cu_2(MoO_4)_3$ are divided into the "intrachain" paths (i.e., J_1, J_1', J_2, and J_2') and the "interchain" paths (i.e., J_3, J_3', J_4, and J_4') (Figure 4c). The spin dimers for the intrachain paths are shown in Figure 5 and those for the interchain paths in Figure 6. The geometrical parameters associated with these paths are summarized in Table 1.

The $(\Delta\epsilon)^2$ values calculated for the spin-exchange paths of $Rb_2Cu_2(MoO_4)_3$ are listed in Table 1 and so are their relative values. The two strongest AFM interactions are the interchain SSE interactions J_3 and J_3', and the next two strongest AFM interactions are the intrachain SSE interactions J_2 and J_2'. According to these four interactions, the Cu^{2+} ions at the Cu(1) sites form a spin ladder defined by

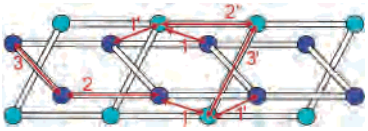

Figure 7. Spin-lattice model for the $[Cu_2(MoO_4)_3]^{2-}$ chains of $Rb_2Cu_2(MoO_4)_3$, which consists of two weakly interacting spin ladders with spin frustration. One spin ladder is based on the Cu^{2+} ions located at the Cu(1) sites and the other spin ladder on those located at the Cu(2) sites. The numbers 1, 1′, 2, 2′, 3, and 3′ refer to the spin-exchange paths J_1, J_1', J_2, J_2', J_3, and J_3', respectively.

the leg interaction $J_{||}$ and the rung interaction $J_\perp$ (i.e., $J_{||} = J_2$, $J_\perp = J_3$, and $J_\perp/J_{||} = 2.50$) and so do those at the Cu(2) sites (i.e., $J_{||} = J_2'$, $J_\perp = J_3'$, and $J_\perp/J_{||} = 1.32$) (Figure 7). These two ladders interpenetrate and interact via the intrachain SE interactions J_1 and J_1', which lead to geometric spin frustration.[22] (The interactions J_4 and J_4' are weak and can be neglected from our discussion.) It is known that a spin ladder made up of spin $^1/_2$ ions has a spin gap[23] and so does an isolated AFM dimer.[24] Thus, it is not surprising that the magnetic susceptibility of $Rb_2Cu_2(MoO_4)_3$ exhibits a maximum. The dominant interactions of the two spin ladders are the rung interactions J_3 and J_3'. The two spin ladders are considerably different (i.e., one with $J_\perp/J_{||} = 2.50$ and the other with $J_\perp/J_{||} = 1.32$). The leg and rung spin-exchange parameters of these two spin ladders are estimated in section 6.

4. Spin Lattice of $BaCu_2V_2O_8$

The description of the crystal structure of $BaCu_2V_2O_8$,[12] i.e., $BaCu_2(VO_4)_2$, is facilitated by considering a CuO_4 chain of cis-edge-sharing, axially elongated CuO_6 octahedra. This is illustrated in Figure 8a, where the two long Cu−O bonds

(21) Clementi, E.; Roetti, C. *At. Data Nucl. Data Tables* **1974**, *14*, 177.
(22) (a) Greedan, J. E. *J. Mater. Chem.* **2001**, *11*, 37. (b) Dai, D.; Whangbo, M.-H. *J. Chem. Phys.* **2004**, *121*, 672.
(23) Barnes, T.; Dagotto, E.; Riera, J.; Swanson, E. S. *Phys. Rev. B* **1993**, *47*, 3196.
(24) Kahn, O. *Molecular Magnetism*: VCH: New York, 1993.

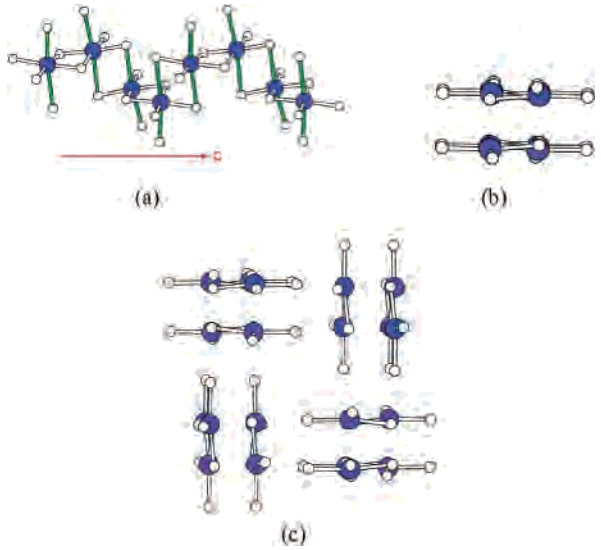

Figure 8. Building blocks of $BaCu_2V_2O_8$: (a) perspective view of a cis-edge-sharing CuO_4 chain, where the two long Cu−O bonds of each CuO_6 octahedron are represented by green cylinders; (b) projection view of a cis-edge-sharing CuO_4 chain after removal of the two long Cu−O bonds of each CuO_6 octahedron, which consists of two $Cu_2(O_{eq})_6$ dimer chains; (c) projection view of how the $Cu_2(O_{eq})_6$ dimer chains are packed in $BaCu_2V_2O_8$. The blue and white circles represent the Cu and O atoms, respectively.

of each CuO_6 octahedron are indicated by green cylinders. Once these bonds are removed, it is seen that each CuO_4 chain consists of $Cu_2(O_{eq})_6$ dimers made up of edge-sharing $Cu(O_{eq})_4$ square planes. A projection view of such $Cu_2(O_{eq})_6$ dimers in one CuO_4 chain along the chain direction is given in Figure 8b, which shows two sets of $Cu_2(O_{eq})_6$ dimers nearly parallel to each other. Each set of nearly coplanar $Cu_2(O_{eq})_6$ dimers forming a chain will be referred to as a $Cu_2(O_{eq})_6$ dimer chain. In $BaCu_2V_2O_8$, the $Cu_2(O_{eq})_6$ dimer chains are packed as depicted in Figure 8c. There are two nonequivalent V atoms, V(1) and V(2), in $BaCu_2V_2O_8$. In each CuO_4 chain, two $Cu_2(O_{eq})_6$ dimer chains are bridged by $V(1)O_4$ and $V(2)O_4$ tetrahedra, as shown in Figure 9a. The $V(1)O_4$ tetrahedra bridge the terminal O_{eq} atoms of the $Cu_2(O_{eq})_6$ dimers within each $Cu_2(O_{eq})_6$ dimer chain and also between $Cu_2(O_{eq})_6$ dimer chains. The $V(2)O_4$ tetrahedra bridge only the shared-edge O_{eq} atoms of the $Cu_2(O_{eq})_6$ dimers between the $Cu_2(O_{eq})_6$ dimer chains.

Sakurai et al.[13] found that the magnetic susceptibility of $BaCu_2V_2O_8$ is characteristic of an alternating Heisenberg AFM chain model

$$\hat{H} = -J_1\sum_i \hat{S}_{2i-1}\cdot\hat{S}_i - J_2\sum_i \hat{S}_{2i}\cdot\hat{S}_{2i+1} \qquad (3)$$

with J_1 much stronger than J_2. However, the spin-exchange paths responsible for J_1 and J_2 were not identified. He et al.[14] showed that the magnetic susceptibility is well reproduced by a strongly alternating AFM chain model with $J_1/k_B = -260$ K and $J_2/k_B = -52$ K and that the high degree of alternation, $\alpha = J_2/J_1 = 0.20$, results in a large spin gap (~230 K). They proposed that the J_1 and J_2 paths occur within a $Cu_2(O_{eq})_6$ dimer chain; i.e., J_1 is the SSE path with the $V(1)O_4$ bridge, and J_2 is the SE path within a $Cu_2(O_{eq})_6$ dimer (Figure 10a). The ^{51}V NMR study of Ghoshray et al.[15]

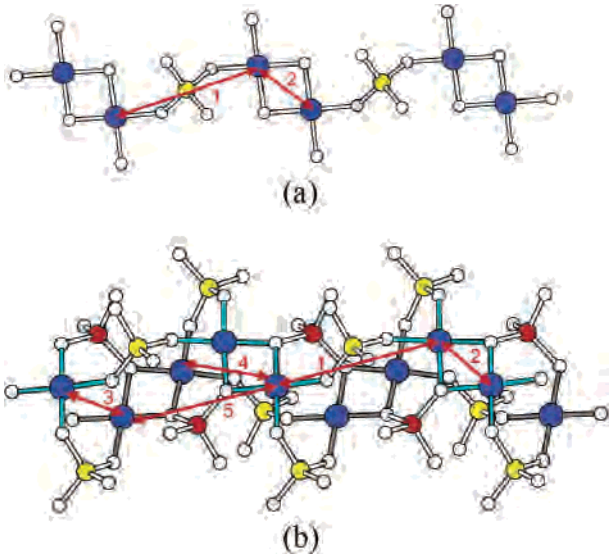

Figure 10. Spin-exchange paths of $BaCu_2V_2O_8$: (a) the two paths proposed by He et al.[11] as forming an alternating AFM chain model; (b) the various spin-exchange paths within each $Cu_2(O_{eq})_6$ dimer chain and between adjacent $Cu_2(O_{eq})_6$ dimer chains.

showed that both the V(1) and V(2) sites have nonzero spin densities and that the exchange interaction via the O−V(1)−O bridge is stronger than that via the O−V(2)−O bridge. This work indicates the involvement of both O−V(1)−O and O−V(2)−O bridges in the spin-exchange interactions not only between the Cu^{2+} ions within each $Cu_2(O_{eq})_6$ dimer chain but also between adjacent $Cu_2(O_{eq})_6$ dimer chains. From their ^{51}V NMR study, Lue and Xie[16] suggested that a nearly

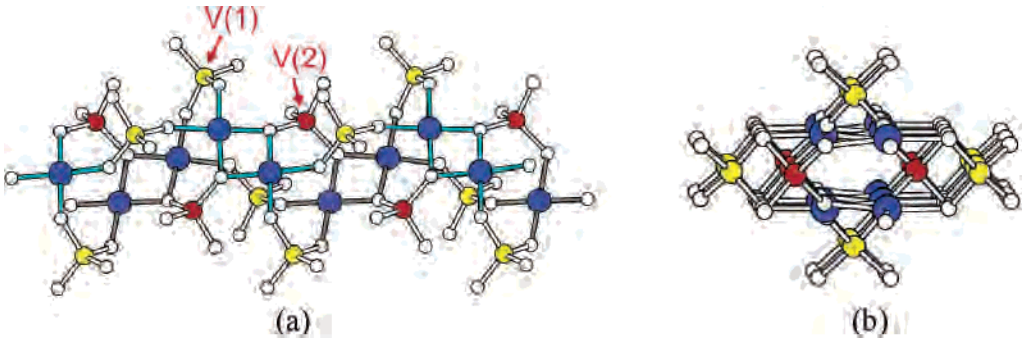

Figure 9. (a) Perspective and (b) projection views of how the two $Cu_2(O_{eq})_6$ dimer chains of a cis-edge-sharing CuO_4 are bridged by $V(1)O_4$ and $V(2)O_4$ tetrahedra in $BaCu_2V_2O_8$. The yellow and red circles represent the V(1) and V(2) atoms, respectively. In part a, the Cu−O_{eq} bonds of the two different $Cu_2(O_{eq})_6$ dimer chains are colored differently to accentuate their difference.

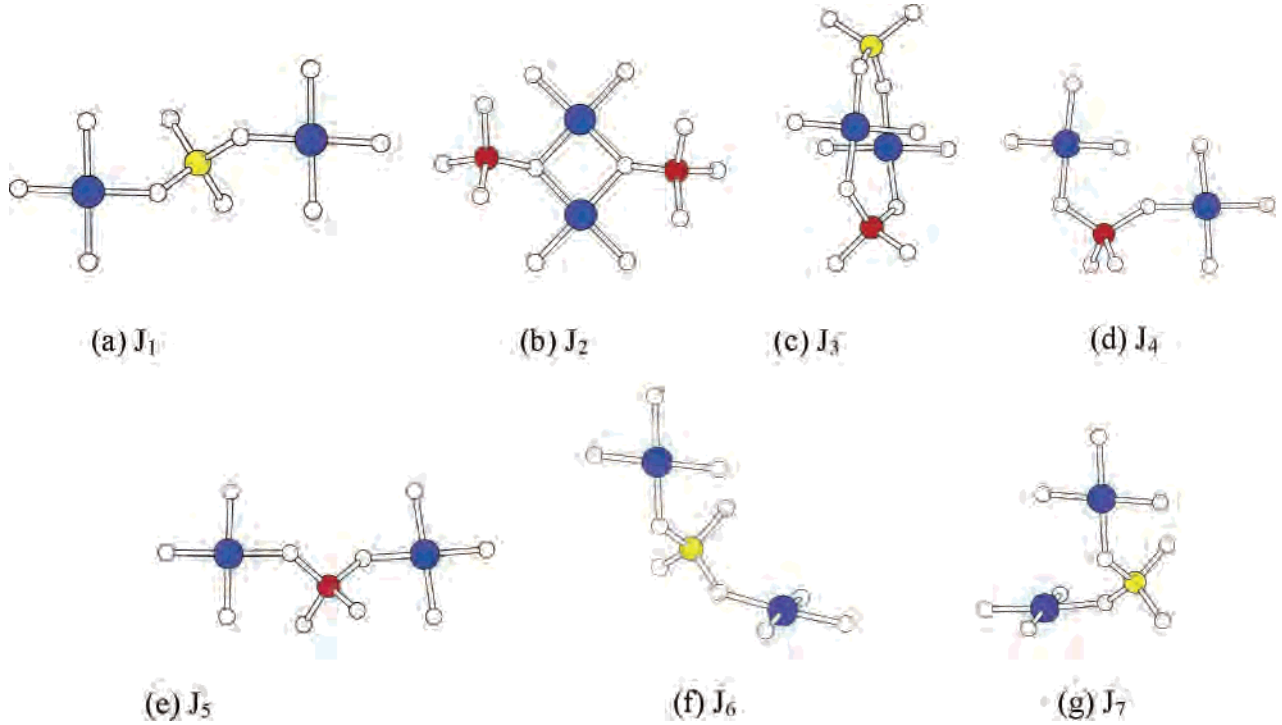

Figure 11. Spin dimers of $BaCu_2V_2O_8$ associated with the spin-exchange paths (a) J_1, (b) J_2, (c) J_3, (d) J_4, (e) J_5, (f) J_6, and (g) J_7.

Table 2. Geometrical Parameters and $(\Delta\epsilon)^2$ Values Associated with the Spin-Exchange Paths in $BaCu_2V_2O_8$[a]

(a) SE Interaction			
path	Cu···Cu	∠Cu−O−Cu	$(\Delta\epsilon)^2$
J_2	2.862	93.7	4750 (0.16)

(b) SSE Interactions				
path	Cu···Cu	O···O	∠Cu−O···O	$(\Delta\epsilon)^2$
Within a Dimer Chain				
J_1	6.314	2.750	142.4, 124.4	20 (0.00)[d]
Between Dimer Chains within a CuO_4 Chain				
J_3	3.007	2.763[b]	93.4, 93.4[b]	28 900 (1.00)
		3.011[c]	89.2, 89.2[c]	
J_4	5.051	3.011	89.2, 147.2	220 (0.01)
J_5	6.614	3.011	147.2, 147.2	10 (0.00)
Between CuO_4 Chains				
J_6	5.841	2.726	142.9, 140.9	570 (0.02)
J_7	5.177	2.806	134.3, 104.2	210 (0.01)

[a] The bond lengths are in Å units, the bond angles are in degrees, and the $(\Delta\epsilon)^2$ values are in $(meV)^2$ units. [b] The Cu−O−V(1)−O−Cu bridge with Cu−O = 1.970 Å. [c] The Cu−O−V(2)−O−Cu bridge with Cu−O = 1.983 Å. [d] The relative values of $(\Delta\epsilon)^2$ are given in parentheses.

isolated dimer model (i.e., $\alpha \approx 0.1$) could be an alternative explanation for the occurrence of a large spin gap in $BaCu_2V_2O_8$.

As was already pointed out, there are two spin-exchange interactions J_1 and J_2 to consider for a $Cu_2(O_{eq})_6$ dimer chain (Figure 10a). Between two $Cu_2(O_{eq})_6$ dimer chains within a CuO_4 chain, one needs to consider the interactions J_3, J_4, and J_5 (Figure 10b). Though not shown, there occur spin-exchange interactions (J_6 and J_7) between two adjacent CuO_4 chains. The spin dimers associated with the interactions J_1−J_7 are presented in Figure 11, and the geometrical parameters associated with them are summarized in Table 2.

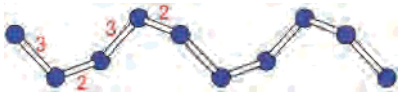

Figure 12. Two spin-exchange paths J_3 and J_2 leading to an alternating AFM chain model for $BaCu_2V_2O_8$, where the numbers 3 and 2 represent the spin-exchange paths J_3 and J_2, respectively.

The $(\Delta\epsilon)^2$ values calculated for the spin-exchange paths of $BaCu_2V_2O_8$ are listed in Table 2 and so are their relative values. The strongest AFM interaction is the SSE interaction J_3, and the second-strongest AFM interaction is the SE interaction J_2. These two interactions form an alternating AFM chain within each CuO_4 chain (Figure 12). The J_2/J_3 ratio (i.e., $\alpha = 0.16$) is small and is consistent with the conclusion from the ^{51}V NMR studies that the alternating chain model is close to an isolated dimer model (i.e., $\alpha = 0.1$,[16] 0.20[14]).

It is of interest to note the nature of the orbital interaction in the spin dimer representing the interaction J_3 (Figure 11c). The two $Cu(O_{eq})_4$ planes are approximately parallel to each other. Thus, in the absence of the O−V−O bridges provided by the $V(1)O_4$ and $V(2)O_4$ tetrahedra, the in-phase and out-of-phase combinations of the their magnetic orbitals (ψ^0_+ and ψ^0_-, respectively) would be practically the same in energy. Consequently, in the absence of the O−V−O bridges, the spin-exchange interaction J_3 would be practically zero, i.e., $(\Delta\epsilon)^2 \approx 0$. In the presence of the O−V−O bridges, however, the out-of-phase combination ψ^0_- interacts with the π-type V 3d orbitals (Figure 13a) but the in-phase combination ψ^0_+ cannot by symmetry (Figure 13b). This introduces an energy split between ψ^0_+ and ψ^0_- and explains why the SSE interaction J_3 is strongly AFM despite the fact that the two magnetic orbitals are nearly eclipsed and parallel to each other. As discussed further in section 6, the symmetry

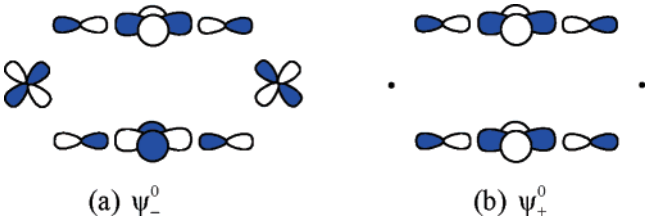

Figure 13. (a) Presence and (b) absence of the bonding interactions of the π-type V 3d orbitals with the magnetic orbitals (ψ_-^0 and ψ_+^0, respectively) in the spin-exchange path J_3 of $BaCu_2V_2O_8$.

of the bridging mode has a strong influence on the strength of an SSE interaction.

It should be noted that the interaction of the magnetic orbitals of the $Cu(O_{eq})_4$ planes with the empty V 3d orbitals of the bridging VO_4 tetrahedra leads to a slight electron transfer (i.e., a slight spin transfer) from the $Cu(O_{eq})_4$ planes to the VO_4 tetrahedra, thereby accounting for why both V(1) and V(2) sites show nonzero spin densities in the ^{51}V NMR experiments. Note that the O−V(1)−O and O−V(2)−O bridges of the spin-exchange path J_3 are not equivalent (Figure 11c and Table 2b). The O−V(1)−O bridges have shorter Cu−O bonds and greater ∠Cu−O···O bond angles than do the O−V(2)−O bridges (Table 2b), so that the V(1) atom has a greater 3d orbital contribution in ψ_-^0 than does the V(2) atom. This is in support of the conclusion from the ^{51}V NMR study[15] that the exchange interaction via the O−V(1)−O bridge is stronger than that via the O−V(2)−O bridge.

5. Spin Lattice of $KBa_3Ca_4Cu_3V_7O_{28}$

The crystal structure of $KBa_3Ca_4Cu_3V_7O_{28}$,[17] i.e., $KBa_3Ca_4Cu_3(VO_4)_7$, is made up of $[Cu_3(VO_4)_7]^{15-}$ clusters. As depicted in Figure 14a,b, each cluster has three $Cu(O_{eq})_4$ square planes arranged to form a hexagonal prism, every two adjacent $Cu(O_{eq})_4$ square planes are bridged by two VO_4 tetrahedra, and one of the three $Cu(O_{eq})_4$ square planes has its axial position capped by one VO_4 tetrahedron. The inverse magnetic susceptibility vs temperature plot of $KBa_3Ca_4Cu_3V_7O_{28}$ shows that the Curie constant changes significantly around 100 K.[18] The Curie constant in the lower temperature region (10−70 K) is smaller compared with that in the higher temperature region (191−250 K) by a factor of 3. The latter indicates that the three Cu^{2+} ions in each $[Cu_3(VO_4)_7]^{15-}$ cluster form a spin lattice of an isolated triangle in which every two neighboring Cu^{2+} ions are antiferromagnetically coupled. The magnetic properties of $KBa_3Ca_4Cu_3V_7O_{28}$ are described by an equilateral-triangle trimer model[18]

$$\hat{H} = -J(\hat{S}_1\cdot\hat{S}_2 + \hat{S}_2\cdot\hat{S}_3 + \hat{S}_3\cdot\hat{S}_1) \quad (4)$$

The analysis of the magnetic susceptibility data using this model shows $J/k_B = -224$ K, which is quite strong. The three Cu^{2+} ions of a $[Cu_3(VO_4)_7]^{15-}$ cluster form an equilateral triangle and have three SSE paths. Although one $Cu(O_{eq})_4$ square plane is capped by a VO_4, the three $Cu(O_{eq})_4$ square planes of a $[Cu_3(VO_4)_7]^{15-}$ cluster are equivalent so that the three SSE paths of the cluster are equivalent. The geometrical parameters and the calculated $(\Delta\epsilon)^2$ value of this SSE path J are summarized in Table 3. The $(\Delta\epsilon)^2$ value is large and hence predicts that the AFM spin exchange J forming an equilateral-triangle model should be strong, in agreement with experiment.[18]

Table 3. Geometrical Parameters and the $(\Delta\epsilon)^2$ Value Associated with the Spin-Exchange Path in $KBa_3Ca_4Cu_3V_7O_{28}$[a]

	Cu···Cu	O···O	∠Cu−O···O	$(\Delta\epsilon)^2$
J	4.227	2.768 2.913	112.4, 112.4 110.1, 110.1	26 500

[a] The bond lengths are in Å units, the bond angles are in degrees, and the $(\Delta\epsilon)^2$ values are in $(meV)^2$ units.

6. Discussion

It is important to compare the spin-exchange path J of $KBa_3Ca_4Cu_3V_7O_{28}$ with the strongest spin-exchange path J_3 of $BaCu_2V_2O_8$. In both paths, the two $Cu(O_{eq})_4$ square planes are bridged by two VO_4 tetrahedra. The J_3/J ratio predicted by the $(\Delta\epsilon)^2$ values is 0.92, which is close to the value of 0.86 determined from the experimental J_3/k_B and J/k_B values (i.e., 224 and 260 K, respectively).[14] In contrast, the strongest spin-exchange interaction of $Rb_2Cu_2(MoO_4)_3$ (Figure 6a) is weaker than that of $BaCu_2V_2O_8$ by a factor of ∼14 [i.e., $(\Delta\epsilon)^2$ = 2080 vs 28900 $(meV)^2$], although the two $Cu(O_{eq})_4$ square planes are bridged by two MoO_4 tetrahedra. It is important to understand why this is the case. In the path J_3 of $BaCu_2V_2O_8$ (Figure 6a) and the path J of $KBa_3Ca_4Cu_3V_7O_{28}$ (Figure 14c), the two $Cu-O_{eq}$ bonds bridged by each VO_4 tetrahedron are oriented such that the magnetic p-orbital tails lying on these two $Cu-O_{eq}$ bonds can overlap well with one π-type V 3d orbital of the VO_4 tetrahedron. In the path J_3 of $Rb_2Cu_2(MoO_4)_3$ (Figure 6a), however, the two $Cu-O_{eq}$ bonds bridged by each MoO_4 tetrahedron are oriented nearly perpendicular to each other so that the magnetic p-orbital tails lying on these two $Cu-O_{eq}$ bonds cannot overlap well

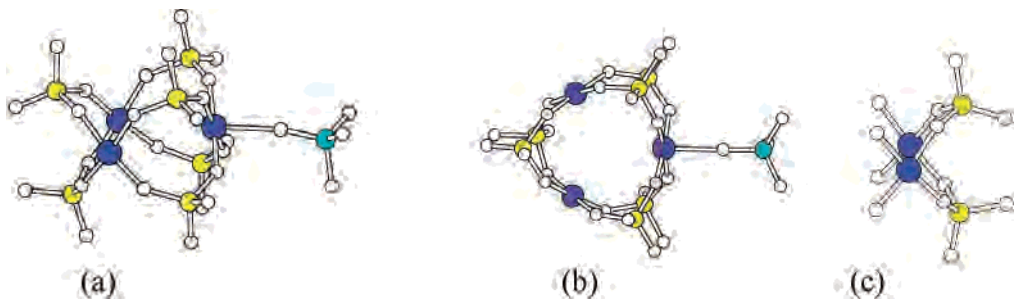

Figure 14. Two views of a $[Cu_3(VO_4)_7]^{15-}$ cluster of $KBa_3Ca_4Cu_3(VO_4)_7$ (a and b) and a spin dimer of a $[Cu_3(VO_4)_7]^{15-}$ cluster (c).

with one π-type Mo 4d orbital of the MoO_4 tetrahedron. This explains why the strongest spin-exchange path J_3 of $Rb_2Cu_2(MoO_4)_3$ (Figure 6a) leads to a much weaker interaction than does that of $BaCu_2V_2O_8$. Thus, the magnitude of an SSE interaction is strongly influenced by the symmetry of the bridging mode. This was also found for the phosphates α-$AgCuPO_4$ and β-$AgCuPO_4$.[7]

The above comparison suggests that the spin-exchange parameter J_3 of $Rb_2Cu_2(MoO_4)_3$ is about -18 K (i.e., 260/14 K). By scaling this value in terms of the relative $(\Delta\epsilon)^2$ values of J_2, J_3, J_2', and J_3', one can estimate the rung and leg spin-exchange parameters of the two spin ladders of $Rb_2Cu_2(MoO_4)_3$. They are $J_{\parallel}/k_B \approx -7$ K and $J_{\perp}/k_B \approx -18$ K for the spin ladder of the Cu(1) sites and $J_{\parallel}/k_B \approx -11$ K and $J_{\perp}/k_B \approx -15$ K for the spin ladder of the Cu(2) sites. To a first approximation, the magnetic properties of $Rb_2Cu_2(MoO_4)_3$ may be described in terms of these two spin ladders without considering their weak interactions.

7. Concluding Remarks

Our spin dimer analysis for $Rb_2Cu_2(MoO_4)_3$, $BaCu_2V_2O_8$, and $KBa_3Ca_4Cu_3V_7O_{28}$ shows that the O−M−O bridges (M = V^{5+}, Mo^{6+}) between the Cu^{2+} ions, provided by the MO_4 tetrahedra, are essential for determining the spin-lattice models needed to interpret the magnetic properties of these oxides. A uniform chain model with nearest-neighbor FM and next-nearest-neighbor AFM interactions proposed for $Rb_2Cu_2(MoO_4)_3$ is not supported. The relevant model is two interpenetrating spin ladders that interact weakly with spin frustration. In both spin ladders, the rung spin exchange $J_{\perp}$ is stronger than the leg spin exchange $J_{\parallel}$ and is associated with the SSE path in which two noncoplanar, nearly parallel $Cu(O_{eq})_4$ square planes are bridged by two MoO_4 tetrahedra. Our study supports the strongly alternating AFM chain model with $\alpha \approx 0.10-0.20$ proposed for $BaCu_2V_2O_8$, but the spin-exchange paths responsible for this model differ from those proposed. The strongest spin-exchange interaction of $BaCu_2V_2O_8$ is related to the SSE path in which two nearly eclipsed, nearly parallel $Cu(O_{eq})_4$ square planes are bridged by two VO_4 tetrahedra. As expected, the spin-lattice model of $KBa_3Ca_4Cu_3V_7O_{28}$ is an equilateral triangle with strong AFM coupling. In the strongest spin-exchange paths of $Rb_2Cu_2(MoO_4)_3$ and $BaCu_2V_2O_8$ as well as in the spin-exchange path of $KBa_3Ca_4Cu_3V_7O_{28}$, the two $Cu(O_{eq})_4$ square planes are bridged by two MO_4 tetrahedra (M = V^{5+}, Mo^{6+}). With respect to the strongest spin exchange of $BaCu_2V_2O_8$, the spin exchange of $KBa_3Ca_4Cu_3V_7O_{28}$ is only slightly weaker, in reasonable agreement with experiment, while the strongest spin exchange of $Rb_2Cu_2(MoO_4)_3$ is much weaker. This difference in the spin-exchange strengths originates from the difference in how the two $Cu(O_{eq})_4$ square planes are bridged by the MO_4 tetrahedra in the spin dimers.

Acknowledgment. The research was supported by the Office of Basic Energy Sciences, Division of Materials Sciences, U.S. Department of Energy, under Grant DE-FG02-86ER45259.

Supporting Information Available: Table S1 of the atomic orbital parameters employed for our EHTB calculations. This material is available free of charge via the Internet at http://pubs.acs.org.

IC060392W